

## ARTICLE OPEN



# Understanding radiation-thermal aging of polydimethylsiloxane rubber through molecular dynamics simulation

Weitao Lou<sup>1</sup>, Chaoyang Xie<sup>2</sup> and Xuefei Guan<sup>1</sup>✉

The effect of radiation-thermal aging on the structure and properties of polydimethylsiloxane (PDMS) rubber at the micro-scale was investigated through molecular dynamics simulation. The aged PDMS models were constructed by incorporating the aging-induced chemical changes (hydroxyl groups, cross-linking, and scission of main chain). The simulation results show that the introduction of hydroxyl groups and cross-linking in molecular chains lower the chain mobility and the diffusion of the chains and oxygen molecules owing to the strong intermolecular interactions and long-chain structure, respectively. The introduction of short chains caused by the scission of main chains can enhance the mobility, diffusion, and flexibility of the chains and the diffusion range of oxygen molecules, resulting in the decrease in the free volume and  $T_g$ . In addition, the hardening effect of cross-linking and the softening effect of scission of main chain collectively contribute to the degradation of mechanical properties of the PDMS rubber.

*npj Materials Degradation* (2022)6:84; <https://doi.org/10.1038/s41529-022-00299-1>

## INTRODUCTION

Polydimethylsiloxane (PDMS) rubber has been widely used as the support cushion, coating, and thermal/electrical insulation, due to its outstanding thermal resistance, and superb electrical and chemical stability<sup>1–3</sup>. In some applications in the field of aerospace and nuclear industries, PDMS rubber is often exposed to radiation, elevated temperature, and oxygen<sup>4</sup>. Radiation, especially gamma rays, can lead to the formation of chain scission, additional cross-linking, and radical<sup>5</sup>. The additional cross-links are formed via the radical (radiation-induced silicon radical, methylene radical, and terminal oxygen radical) coupling reactions<sup>6</sup>. In addition, the presence of oxygen ( $O_2$ ) and elevated temperature further promote the degradation process by propagating oxidation reactions, such as oxidative cross-linking and chain scission and the formation of oxidation products and oxidation radicals<sup>7</sup>. The radiation and thermal oxidation-induced chemical reactions can alter or degrade many properties including network structure, permanent set, and Young's modulus<sup>8</sup>. Thus, it is necessary to explore the synergistic effect of radiation and thermal oxidation on the chemical structure and properties of PDMS rubber.

Recently, research work on the aging behaviors and mechanisms of PDMS rubber exposed to radiation, temperature, and mechanical load has been reported, especially on the coupling effect of radiation and other environmental factors<sup>7,9–11</sup>. The quantitative analysis of the chemical reaction was conducted by Fourier transform infrared spectroscopy (FTIR)<sup>12,13</sup>, nuclear magnetic resonance (NMR) measurement<sup>14</sup>, thermogravimetric analysis (TGA)<sup>15</sup>, and pyrolysis gas chromatography-mass spectrometry (Py-GC/MS)<sup>16</sup>, etc. The types of aging products, such as cross-linking and chain scission, during the aging process were indirectly identified by these experimental measures<sup>17,18</sup>. However, it is highly nontrivial to infer the effect of fundamental chemical events on the network structure and dynamics properties of the PDMS rubber. In the current scenario, molecular dynamics (MD) simulation can provide useful insights into the

structure–performance relationships of polymer materials<sup>19,20</sup>. It is particularly well-suited to study the radiation and thermal-induced chemical effects at the molecular level. Nevertheless, few works have focused on the effect of radiation and thermal damage on the microstructure and properties of PDMS rubber at micro scale<sup>21,22</sup>. For example, Kroonblawd et al.<sup>21</sup> applied ensembles of quantum-based molecular dynamics (QMD) simulations to predict the radiation damage of polydimethylsiloxane. They revealed the changes in radiation-induced network including the formation of branch points, carbon linkages, and bond scission. Liu et al.<sup>22</sup> studied the  $\gamma$  radiation-induced chemical reactions and physico-chemical interactions by reactive molecular dynamics (ReaxFF MD) simulations. They showed that main chains, gas products, radical reactive species, and silica fillers were the polyfunctional participants. Therefore, the investigation on the effect of radiation and thermal-induced chemical changes on the structure and properties of PDMS rubber by leveraging advantage of MD simulation is still warranted.

In this study, the radiation-thermal aging effect of PDMS rubber on the structure and properties was investigated by MD simulation. Molecular models of unaged and aged PDMS were constructed by incorporating radiation and thermal-induced chemical changes including the formation of oxidation product, cross-linking, and scission of the main chain. After that, the MD simulations were performed. Critical parameters, such as density, fractional free volume (FFV), hydrogen bonds (H-bonds), mean square displacement (MSD) and self-diffusion coefficients, radius of gyration, glass transition temperature, and mechanical properties (stress–strain curves) of the unaged and aged molecular models were extracted to aid the understanding of the influences of radiation and thermal-induced chemical changes on the structure and properties of PDMS rubber. In addition, the effects of aging-induced chemical changes on diffusion behaviors of  $O_2$  molecules in the PDMS matrix were estimated by MSD, diffusion coefficients and trajectories of  $O_2$  molecules.

<sup>1</sup>Graduate School of China Academy of Engineering Physics, Beijing, China. <sup>2</sup>Institute of Systems Engineering, China Academy of Engineering Physics, Mianyang, China. ✉email: xfguan@gscaep.ac.cn

## RESULTS AND DISCUSSION

### Density

The simulated densities of the unaged and aged PDMS models were obtained by a 500 ps NPT simulation at 101 kPa and 298 K. Figure 1 shows the changes in the densities of the unaged and aged PDMS models as a function of simulation time. The average densities of the unaged and aged PDMS models are shown in Fig. 2. About 2% fluctuations of the simulated densities for all the PDMS models can be observed during the simulation process, which implies that each of the systems has reached the equilibrium. The predicted average density of the unaged PDMS model is  $0.9952 \text{ g cm}^{-3}$ , which is close to the actual densities ( $0.95\text{--}0.98 \text{ g cm}^{-3}$ )<sup>23–25</sup>. The results indicate the constructed rubber packing models can be used to represent the actual materials to a certain extent. It can be found that the PDMS model presents a slight increase in density along with the introduction of radiation and thermal-induced chemical changes. The increase in density during the aging process is mainly due to the formation of oxidation products and cross-links.

### Fractional free volume (FFV)

The free volume is often employed to evaluate the packing structure of polymeric systems and permeate behavior of gas molecules in the material. The FFV value of the unaged and aged

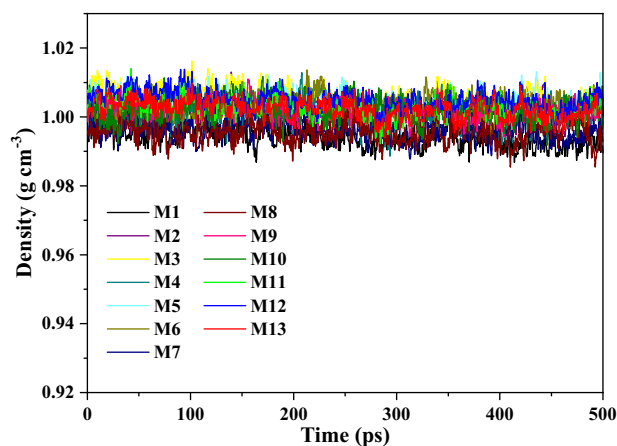


**Fig. 1** Density of the unaged and aged PDMS models as a function of simulation time.

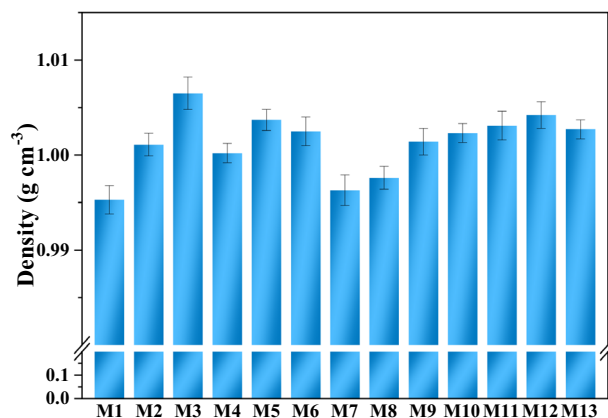
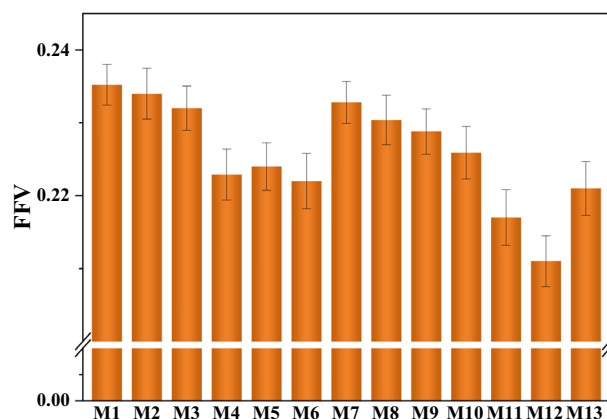


**Fig. 2** The average densities of the unaged and aged PDMS models. The error bars stand for the standard deviations from five independent sample.

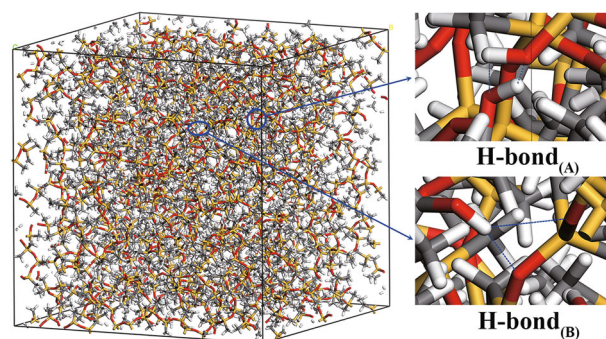
PDMS models can be calculated by the following equation<sup>26</sup>.

$$\text{FFV} = 1 - \frac{V_0}{V_S}, \quad (1)$$

where  $V_0$  and  $V$  correspond to the occupied volume and the specific volume of the unaged and aged PDMS chains, respectively. The FFV was then quantitatively determined using a probing spherical particle with a radius equivalent to the Van der Waals radius of oxygen molecules ( $1.438 \text{ \AA}$ )<sup>27</sup> to test whether a volume can be accessible. Therefore, the value of Connolly radius is set as  $1.438 \text{ \AA}$ . Figure 3 shows the FFVs of the unaged and aged PDMS models. The FFVs of the M2 and M3 models show a slight decrease, indicating that the introduction of hydroxyl groups leads to the reduction of the free volume. The introduction of hydroxyl groups in molecular chains contributes to the increase of strong polar interactions including non-bonded interaction and hydrogen bonds between molecular chains, and therefore reducing the free volume. Figure 4 shows the types of H-bonds in the M3 model. The formation of the first H-bond (A) or O–H...O is between the hydroxyl group (Si–OH and Si–CH<sub>2</sub>–OH) and the hydroxyl group (Si–OH and Si–CH<sub>2</sub>–OH). The formation of the second H-bond (B) or O–H...O is between the hydroxyl group (Si–OH and Si–CH<sub>2</sub>–OH) and the oxygen from the Si–O–Si main chain. The types and numbers of H-bonds in different aged PDMS models were obtained by MD simulations and listed in Table 1. In this study, two molecules are chosen as being hydrogen only if their inter-oxygen distance is less than  $2.7 \text{ \AA}$ , and simultaneously the O–H...O angle is more than  $90^\circ$ <sup>28,29</sup>. The results indicate that the probability of the formation of the hydrogen bonds will increase with the increasing hydroxyl group. An obvious decrease in FFV is observed in the M4, M5, M6, M11, and M12 models, which implies that the cross-linking of the main chain reduces the FFV. The FFV



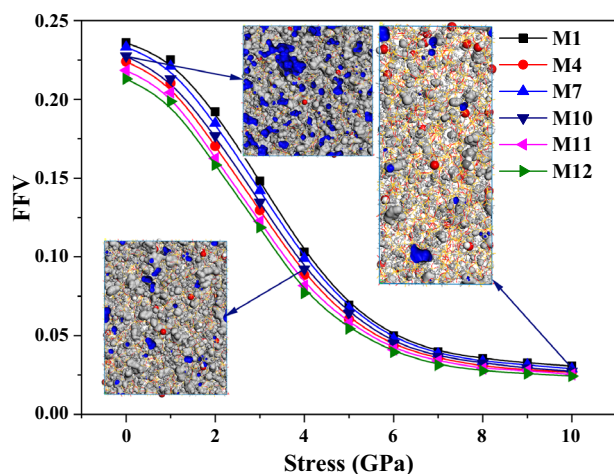
**Fig. 3** FFVs of the unaged and aged PDMS models. The error bars stand for the standard deviations from five independent sample.



**Fig. 4** The types of H-bonds in the M3 model.

**Table 1.** The types and numbers of H-bonds in different PDMS models.

PDMS model	M1	M2	M3	M7	M8	M9	M10	M13
No. of H-bond <sub>(A)</sub>	0	2	5	1	0	0	0	0
No. of H-bond <sub>(B)</sub>	0	8	12	4	3	4	2	2
No. of total H-bonds	0	10	17	5	3	4	2	2

**Fig. 5** FFVs of the unaged and aged PDMS models under different stress levels. The blue and gray regions in the insets represent the free volume and the occupied volume, respectively.

values of the M4, M5, and M6 models present a relatively small difference. The reason for these phenomena is that the formation of the cross-linking structures significantly limited the free motion of molecular chains. Nevertheless, the type of cross-link plays a similar influence on the free volume of the PDMS system. In addition, a slight decrease of FFV can be observed in the M7 and M8 models, which means that the scission of the Si–O–Si main chain results in the decrease of free volume. Furthermore, The FFVs of the M9 and M10 models are greater than that of the M4, M5, and M6 models. The changes in FFV of M9 and M10 models are attributed to the coupling effect of hydroxyl groups, cross-linking and chain scission. The lower FFV value makes it harder for outside molecules (especially O<sub>2</sub>) to diffuse into the aged PDMS models, which may further lower the aging rate.

The FFVs of the typical unaged and aged PDMS models under different temperatures and stress levels were calculated to investigate the effect of temperature and stress. Figure 5 presents the free volume distribution of four arbitrarily chosen models under different stress levels. The blue and gray regions in the inset figures correspond to the free volume and the occupied volume, respectively. The FFVs show a rapid decrease in the stress range of 0 and 6 GPa, and decrease slowly in the range of 6 to 10 GPa. This phenomenon can be explained by the fact that the increase of compressive stress gradually compresses the interstitial spaces in the network structure and inhibits the thermal movement of molecular chains, and the process reaches a balanced state when the stress is large enough.

#### Mean square displacement and self-diffusion coefficients

The mean square displacement (MSD) is widely used to describe the mobility of segmental molecules and particles, which can reveal the relaxation behavior of molecular chains. The self-diffusion coefficients ( $D_s$ ) are one of the critical parameters in

quantitatively characterizing the mobility of the polymer chains and particles. The  $D_s$  can be calculated by the Einstein equation<sup>26</sup>.

$$D_s = \frac{1}{6N} \lim_{t \rightarrow \infty} \frac{d}{dt} \sum_{i=1}^N \langle |r_i(t) - r_i(0)|^2 \rangle, \quad (2)$$

where  $N$  is the number of atoms in the main chain,  $r_i(0)$  and  $r_i(t)$  represent the position of atom  $i$  at time 0 and  $t$ , respectively,  $\langle |r_i(t) - r_i(0)|^2 \rangle$  is the mean square displacement (MSD) of the participating atoms in the course from time 0 to time  $t$ <sup>30</sup>. Figure 6a, b present the MSD results of the main chain in the unaged and aged PDMS models and oxygen of the hydroxyl group in oxidative-aging models as a function of simulation time, respectively. Figure 7a, b shows the  $D_s$  of the main chain and oxygen of the hydroxyl group in PDMS models, respectively.

The results show that the MSD and  $D_s$  of M7 and M8 models are larger than that of the unaged PDMS model (M1), which can be attributed to the fact that the scission of the Si–O–Si main chain improves the mobility and diffusion of molecular chains due to the formation of short chains during aging. The MSD and  $D_s$  of M2 and M3 models are slightly lower than that of the M1 model, indicating that the introduction of hydroxyl groups decreases the mobility and the diffusion of molecular chains owing to the strong polar interaction between molecular chains. In addition, the M4, M5, and M6 models also show smaller values of MSD and  $D_s$  than that of the M1 model. It is noticeable that the M4, M5, and M6 models have similar values of MSD and  $D_s$ . The MSD of M11 and M12 models are less than that of the M4, M5, and M6 models. These phenomena illustrate that the formation of multiple-chain cross-linking structures decrease chain mobility. The changes in MSD and  $D_s$  of M10 and M13 models are due to the coupled effect of hydroxyl group and cross-linking (including direct cross-linking between chains and cross-linking after the scission of the Si–O–Si main chain). The values of MSD and  $D_s$  of the M9 model are between that of the M3 model and the M4 model, which further implies that the introduction of short chains promotes the mobility and diffusion of molecular chains. The similar behaviors are observed for the MSD and  $D_s$  of oxygen of the hydroxyl group in the M2, M3, M7, M9, M10, and M13, models. The MSD and  $D_s$  of the oxygen of the hydroxyl group are larger than that of the main chain in these models, which may be explained by the faster molecular mobility associated with the side and the end groups.

#### Radius of gyration

The radius of gyration ( $R_g$ ) can be used to describe the flexibility and compactness of the polymer chains. The term  $R_g$  can be calculated by the following equation<sup>31</sup>.

$$R_g = \left( \frac{\sum_i m_i \|r_i\|^2}{\sum_i m_i} \right)^{\frac{1}{2}}, \quad (3)$$

where  $m_i$  is the mass of atom  $i$  and  $r_i$  represents the position of atom  $i$  with respect to the center of the molecule mass. Figure 8 shows the results of  $R_g$  of the unaged and aged PDMS models as a function of time, where relatively stable  $R_g$  values for each of the models were achieved in the 500 ps timeframe of the simulation. The  $R_g$  of the aged PDMS models with oxidized chains (M2 and M3) gradually decreases with the increase in the content of the hydroxyl group, compared with that of the unaged PDMS model. This indicates that the introduction of the hydroxyl groups promotes increases the aggregation of molecular chains due to the strong polar interaction. However, the  $R_g$  values of the M4, M5, M6, M11, and M12 models are smaller than that of the M1 model, implying that the formation of cross-linking structure also leads to the aggregation of the chains. The three types of cross-links have a similar effect on the compactness of chains. In addition, the smallest  $R_g$  value is observed for the M7 model, which may

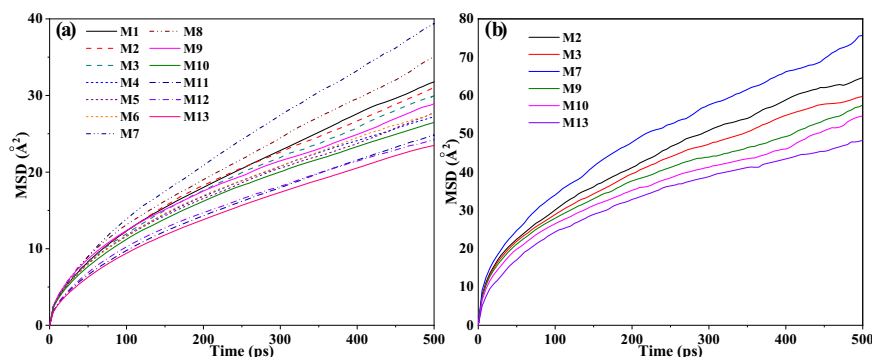


**Fig. 6** MSDs of the unaged and aged PDMS models as a function of simulation time. **a** main chain, and **b** oxygen of hydroxyl group.

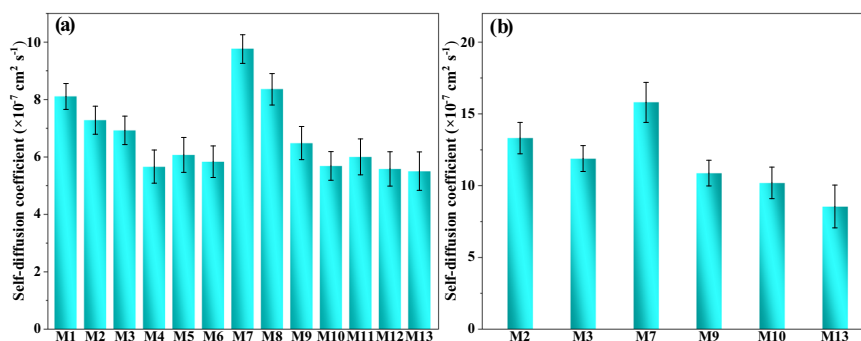


**Fig. 7** Self-Diffusion Coefficient of the unaged and aged PDMS models. **a** main chain and **b** oxygen of hydroxyl group. The error bars stand for the standard deviations from five independent sample. Note that there is no hydroxyl group in modes M1, M4, M5, M6, M8, M11, and M12.

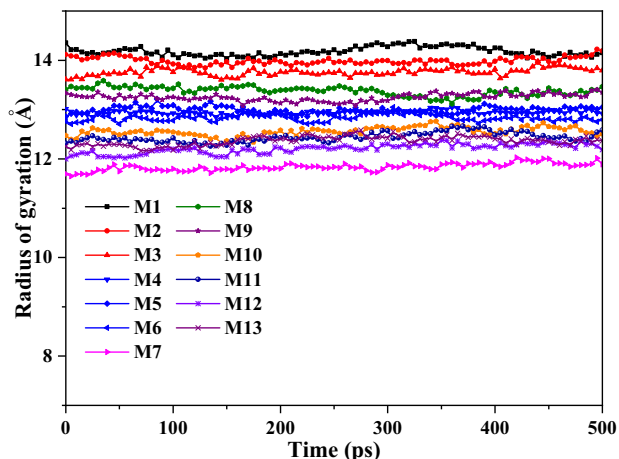


**Fig. 8** The radius of gyration of the unaged and aged PDMS models as a function of simulation time.

indicate that the scission of the main chain greatly enhanced the flexibility of chains. The change in  $R_g$  in the three models of M8, M9, and M10 signifies that cross-linking and chain scission play a more important role in the flexibility and compactness of chains than the formation of hydroxyl groups during the aging process.

### Glass transition temperature ( $T_g$ )

The glass transition temperature,  $T_g$ , is one of the critical parameters of polymers, which characterizes the thermal properties of polymers. The slope of the change in the FFV of the PDMS model with respect to the increasing temperature is relatively small when the temperature is less than the  $T_g$ , due to the frozen

state of polymer chains. However, the FFV rapidly increases with the increasing temperature when the temperature is above  $T_g$ . As the change in the FFV lead to the change in density, an abrupt change in density and specific volume (free volume) is expected to occur at  $T_g$  when the polymer is cooled from a rubbery state to a glassy state<sup>32</sup>. In this work, the change in FFV as a function of temperature is used to estimate  $T_g$  of the unaged and aged PDMS models<sup>33</sup>. Based on the FFV vs. temperature results, the  $T_g$  can be evaluated as the intersection of the two fitted lines of the slope of the change in FFV.

Figure 9 presents the FFV vs. temperature results of the unaged PDMS model. It can be found that the FFVs of the models increase monotonically as the temperature increases. This is mainly because the increasing temperature promotes the free motion of molecular chains and destroys the formation of the hydrogen bond. The  $T_g$  of the unaged PDMS model is evaluated as 183.5 K using the results, which is significantly larger than the experimental results (146–150 K) for the unaged PDMS<sup>34–36</sup>. The deviation can be attributed to the PDMS system without additives and the difference in pressure and temperature between the material production process and MD simulations. Figure 10 shows the  $T_g$  values of models M3, M4, M7, and M10 model, respectively. It can be found that the M3 model has a larger value of  $T_g$  (191.6 K) compared to the M1 model. The main reason is that more hydroxyl groups promote the formation of stronger polar interaction, in particular, the hydrogen bonds, which reduce the chain mobility. In addition, the M4 model has a larger value of  $T_g$  (203.8 K) than the M1 and M2 models, which implies that the cross-linking structures significantly restrict the movement of chains and enhance the thermal stability of the PDMS system, compared to the effect of hydroxyl groups in the M3 model. On the contrary, a smaller value of  $T_g$  (179.2 K) is observed in the M7 model, indicating that the chain scission promotes the chain mobility and lowers the thermal stability of the PDMS system. The

M10 model has the larger value of  $T_g$  (208.3 K) than the M4 model, which is largely attributed to the synergistic effect of hydroxyl groups and cross-linking structures. In addition, the largest  $T_g$  of M12 model (210.2 K) implies the key role of four-chain cross-linking structure during degradation process.

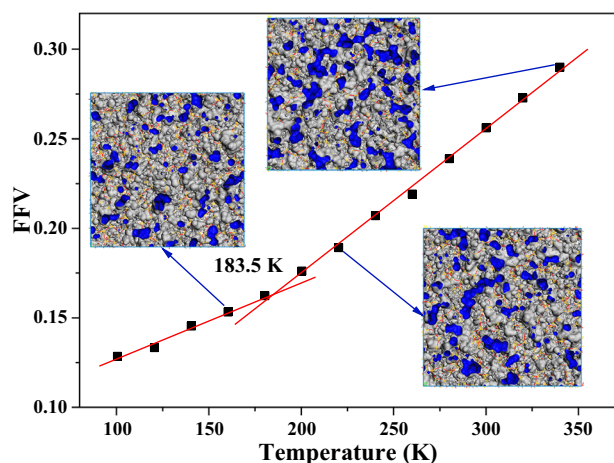


**Fig. 9** The glass transition temperature  $T_g$  of the unaged PDMS model via FFV -temperature dependence.

## Mechanical property

Based on the MD simulation trajectories of the equilibrium structures at 298 K, the constant-pressure method is used to predict the mechanical property by the Souza-Martins barostat<sup>37,38</sup>. The stress-strain curves of the unaged and aged PDMS models were obtained via a series of gradient loading, as shown in Fig. 11. It is noted that the simulation results are much larger than the experimental results of the pure PDMS<sup>39</sup> owing to the difference in the scale between the MD simulation at the atomic level and the experiment at the macro level<sup>40–42</sup>. The micro mechanical properties in the simulation are calculated by analyzing the trajectories including the quality and speed of atoms<sup>43</sup>. It can be observed from Fig. 11 that the results of the simulation and experiment show a similar tendency, which illustrates that the physical and structural evolution of the constructed PDMS model in the simulation fits the mechanism running in the experiment. In addition, the stress rapidly increases during the first stage, followed by a linear regime. No obvious difference in stress response can be observed between the M1 model and the M3 model, which means that the introduction of hydroxyl groups in the M3 model has a limited influence on the mechanical property of the PDMS system. The slope of the stress-strain curves of the M4 and M12 models show a slight increase compared with that of the M1 model, which indicates that the cross-linking improves the stiffness of the PDMS system.

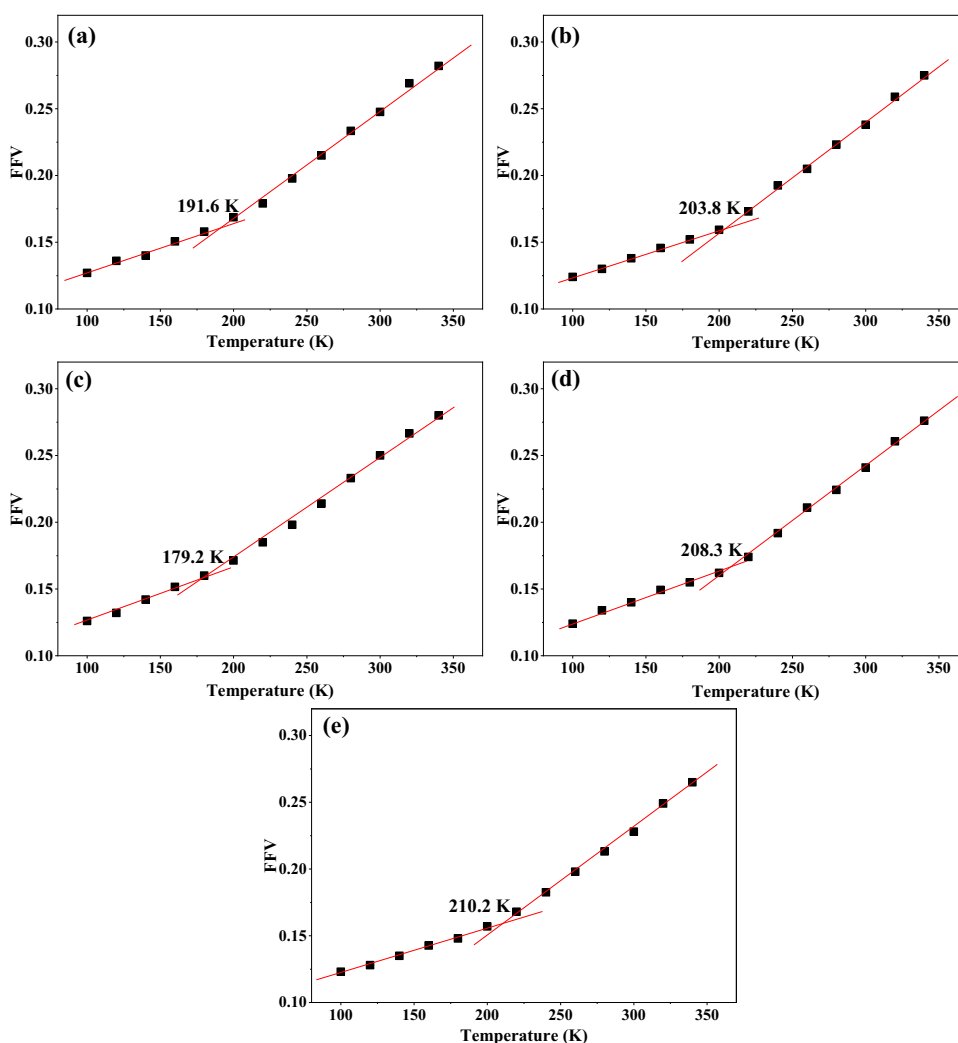


**Fig. 10** Estimated  $T_g$  of the typical aged PDMS models via density vs. temperature results. **a** M3, **b** M4, **c** M7, **d** M10, and **e** M12.

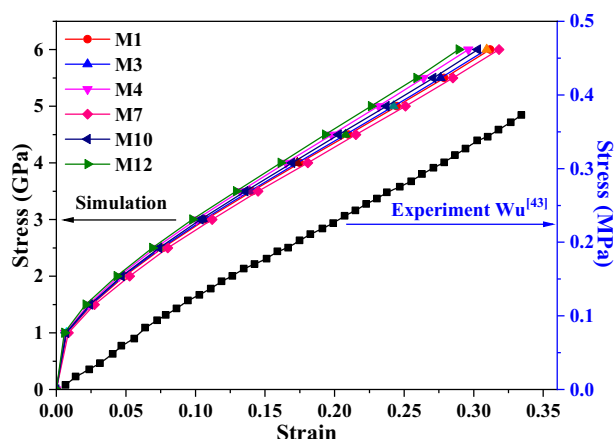


**Fig. 11** Stress-strain curves of the typical unaged and aged PDMS models in simulation and the pure PDMS in experiment.

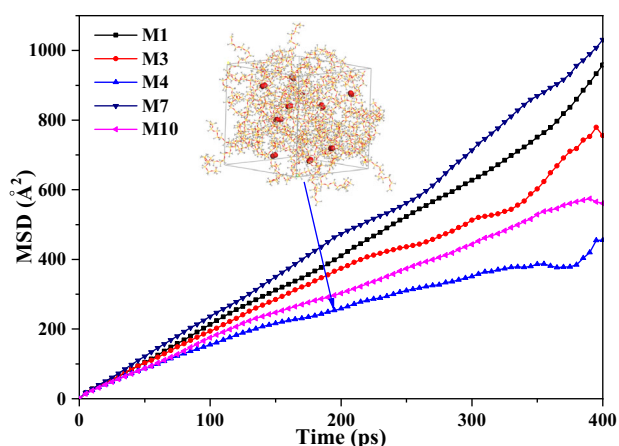


**Fig. 12** MSDs of  $O_2$  molecules in the unaged and aged PDMS models at 298 K as a function of simulation time.

Nevertheless, a small decrease in the slope of the compressive stress-strain curves can be observed in the M7 model. The main reason is that the scission of the main chain forms the short chains resulting in the decrease in reduced mechanical properties. The change in the slope of the compressive stress-strain curves of the M10 model further proves the hardening effect of cross-linking links and the softening effect of chain scission on mechanical properties during the aging process, respectively.

### Diffusion behaviors of oxygen in PDMS

Figures 12 and 13 show the MSDs and diffusion coefficients of  $O_2$  molecules in unaged and aged PDMS models at 298 K, respectively. The results show that the diffusion coefficient of  $O_2$  molecules in unaged PDMS model (M1) is  $3.72 \times 10^{-5} \text{ cm}^2 \text{ s}^{-1}$ , which agrees well with the experimental results  $3.55 \times 10^{-5} \text{ cm}^2 \text{ s}^{-1}$ <sup>44</sup>. The values of the MSDs and diffusion coefficients of  $O_2$  molecules in unaged and aged PDMS models decrease in the following order: M7 > M1 > M3 > M10 > M4. It can be concluded that the introduction of hydroxyl groups and cross-links limits the mobility and the diffusion of  $O_2$  molecules, which is attributed to the strong polar interaction and cross-linking structure, respectively. The formation of the short chains promotes the mobility and the diffusion of  $O_2$  molecules, due to the better flexibility of the low molecular weight chains. In addition, the polar interaction also exists among the oxidized short chains. Therefore, the changes in the MSDs and diffusion coefficients of  $O_2$  molecules are mainly attributed to the

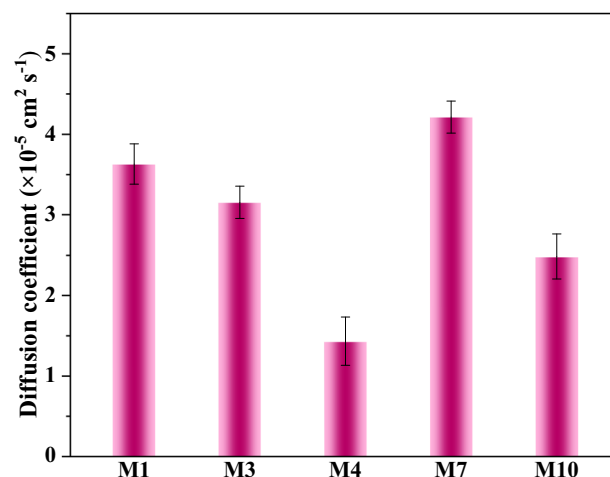


**Fig. 13** Diffusion coefficients of  $O_2$  molecules in the unaged and aged PDMS models at 298 K. The error bars stand for the standard deviations from five independent sample.

competition between the PDMS chains and the oxidized short chains.

To further study the effect of aging-induced chemical changes on the diffusion mechanisms in the unaged and aged PDMS models, the diffusion trajectories of 10  $O_2$  molecules in the M1, M4, M7, and M10 models are obtained and shown in Fig. 14. It can be found that the  $O_2$  molecules show significant motion in the PDMS models during the simulation process. The diffusion of  $O_2$  molecules in the PDMS can occur by a hopping mechanism<sup>45</sup>. The  $O_2$  molecule vibrates inside a microcavity in the PDMS matrix for a period of time, followed by occasional jump into a neighboring microcavity by a tunnel induced by the cooperative motions of the PDMS chains. It should be noted that the diffusion of the  $O_2$  molecules in M1 (Fig. 14a) and M7 (Fig. 14c) models execute more frequent jumps than that of the  $O_2$  molecules in M4 (Fig. 14b) and M10 (Fig. 14d) models, which present more vibrations inside the microcavities. In addition, the lengths of the diffusion trajectories of  $O_2$  molecules in M1 and M7 models are longer than that of the  $O_2$  molecules in M4 and M10 models. These imply that the formation of the cross-linking structures restricts the diffusion of  $O_2$  molecules and reduces the number of jumps and the lengths of jumps. The chain scission enhances the ranges of the diffusion trajectories of  $O_2$  molecules in PDMS matrix, which is attributed to the formation of more tunnels surrounding the microcavities between the short chains.

## METHODS

### Molecular models

Understanding the influence of radiation-thermal aging on the structure and properties of PDMS rubber is necessary to construct the aged molecular models considering aging-induced chemical changes. Previous studies have showed that chemical changes at the atomic-scale during the aging process include breakage/oxidation of side groups, cross-linking, chain scission, and rearrangement, which collectively alter the network structure and degrade the bulk properties of silicon rubber<sup>46–50</sup>. The breakages of side groups ( $\text{Si-CH}_3$  and  $\text{C-H}$  bond in  $\text{CH}_3$ ) form unstable radicals ( $\text{Si-CH}_2\cdot + \cdot\text{H}$  and  $\text{Si}\cdot + \cdot\text{CH}_3$ ), which subsequently react with oxygen to produce peroxy radicals and unstable hydroperoxides. The hydroperoxides decompose into other oxygen-containing radicals ( $\text{Si-O}\cdot$  and  $\text{Si-CH}_2\text{-O}\cdot$ ) and hydroxyl radicals ( $\cdot\text{OH}$ ). In addition, the scission of the  $\text{Si-O-Si}$  main chain also produces unstable radicals ( $\text{Si-O}\cdot$  and  $\text{Si}\cdot$ ), which can react with oxygen. The chemical reactions between these

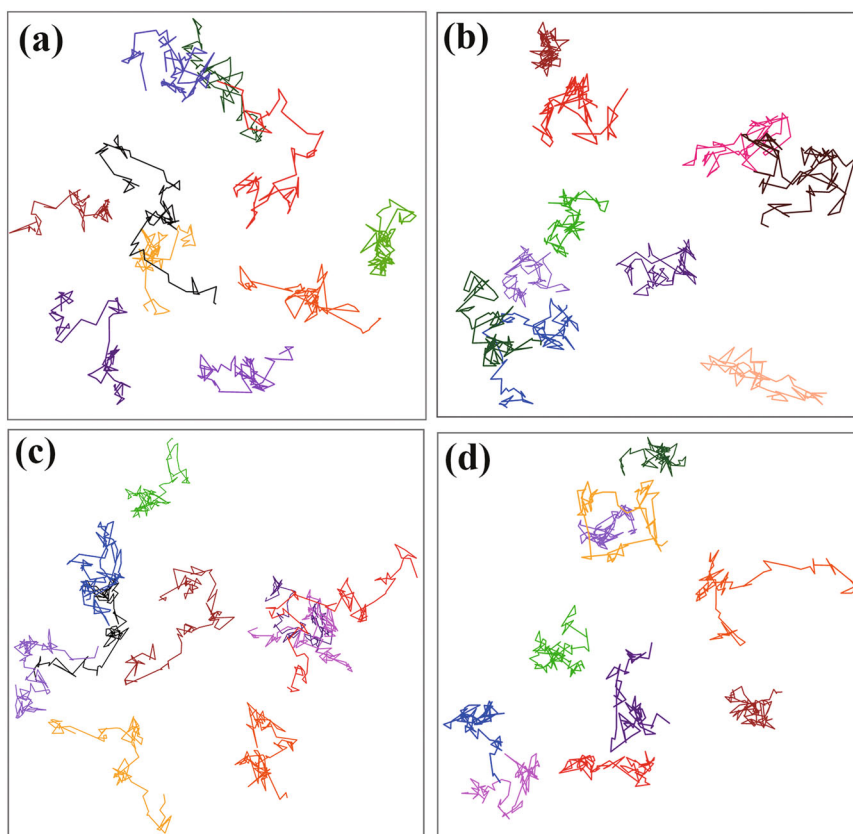


**Fig. 14** The diffusion trajectories of O<sub>2</sub> molecules in the unaged and aged PDMS models. **a** M1, **b** M4, **c** M7, and **d** M10.

unstable radicals further form oxidation products and additional cross-links. The hydroxyl groups (Si-OH and Si-CH<sub>2</sub>-OH) are major oxidation products during the aging process. The additional cross-links include Si-C-C-Si links, Si-C-Si links, Si-O-Si links, etc. Therefore, the oxidized molecular chains with hydroxyl groups, short chains formed by scission of the main chain, and cross-linking structures were constructed based on chemical reactions by Amorphous cell modules using the commercial package Materials Studio, as shown in Fig. 15. Figure 15a shows the typical chemical structure of the PDMS chain including 50 dimethylsiloxane monomers, named chain A. The oxidized PDMS chains (B and C) were constructed by introducing two and four hydroxyl groups (Si-OH and Si-CH<sub>2</sub>-OH), respectively, as shown in Fig. 15b, c, respectively. Figure 15d–f show three types of cross-linking structures of Si-C-Si link (D), Si-O-Si link (E), and Si-C-C-Si link (F), respectively. These links play an important role in the aging of PDMS. The unstable radicals (Si-O• and Si•) due to the scission of Si-O-Si main chain can react with hydrogen radicals to produce stable short chains (Si-OH and Si-H) (Fig. 15g, named chain G) or further combine with other radicals (Si-CH<sub>2</sub>•, Si•, Si-O•, etc) to make the additional cross-links (Fig. 15h, i, named chain H and I), respectively. Additionally, a three-chain cross-linking structure (Fig. 16a, named chain J) and was constructed via Si-O-Si and Si-C-Si links. A four-chain cross-linking structure (Fig. 16b, named chain K) was constructed via Si-O-Si, Si-C-Si, and Si-C-C-Si links.

The geometry optimization was conducted for the unaged and aged PDMS chains by minimizing the system energy for 10,000 steps with an energy convergence value of  $2.0 \times 10^{-5}$  Kcal mol<sup>-1</sup> Å<sup>-1</sup>. After that, the unaged and aged PDMS models were constructed based on these unaged and aged molecular chains, as shown in Table 2. For each PDMS system, five parallel models were randomly generated to obtain the reliable simulation results. The periodic boundary conditions were

employed in the three dimensions of the simulation cubic cell with the random molecular chains. Furthermore, the oxidative-aging reactions between oxygen and PDMS chains depend largely on the diffusion rate of O<sub>2</sub> molecules in the rubber network, which can be affected by the radiation and thermal-induced chemical changes during the aging process. Therefore, the unaged and aged PDMS models (M1, M3, M4, M7, and M10) containing 10 O<sub>2</sub> molecules were constructed to investigate the effect of radiation-thermal aging on diffusion behaviors of O<sub>2</sub> molecules in the PDMS matrix.

#### MD simulation methods

All MD simulations were conducted using the Materials Studio software. The COMPASS (condensed-phase optimized molecule potentials for atomistic simulation studies) force field was employed for describing molecule interactions and intermolecular potential<sup>51</sup>. Atom-based summation method and Ewald summation method were applied for van der Waals interaction and electrostatic interaction during all the simulation processes, respectively. The time step of 1.0 fs was set for all simulations. The MD simulation process is detailed as follows: (1) 10,000 steps of geometry optimization were performed to minimize system energy via the optimization method; (2) 20 cycles of annealing simulation were conducted under NVT (constant number of particles, volume, and temperature), with the temperature ranging from 300 to 500 K; (3) 500 ps NPT simulation was carried out at 300 K and 101 kPa; (4) 500 ps NVT (constant number of particles, pressure, and temperature) simulation was conducted at 300 K to further relax the polymer structure; and (5) 500 ps NPT simulation was carried out at 298 K and 101 kPa to obtain the finally stable structure for analyzing structure and properties of systems. The temperature and pressure were controlled by the Andersen thermostat<sup>52</sup> and Berendsen barostat<sup>53</sup>, respectively. The parameters of density, fractional free

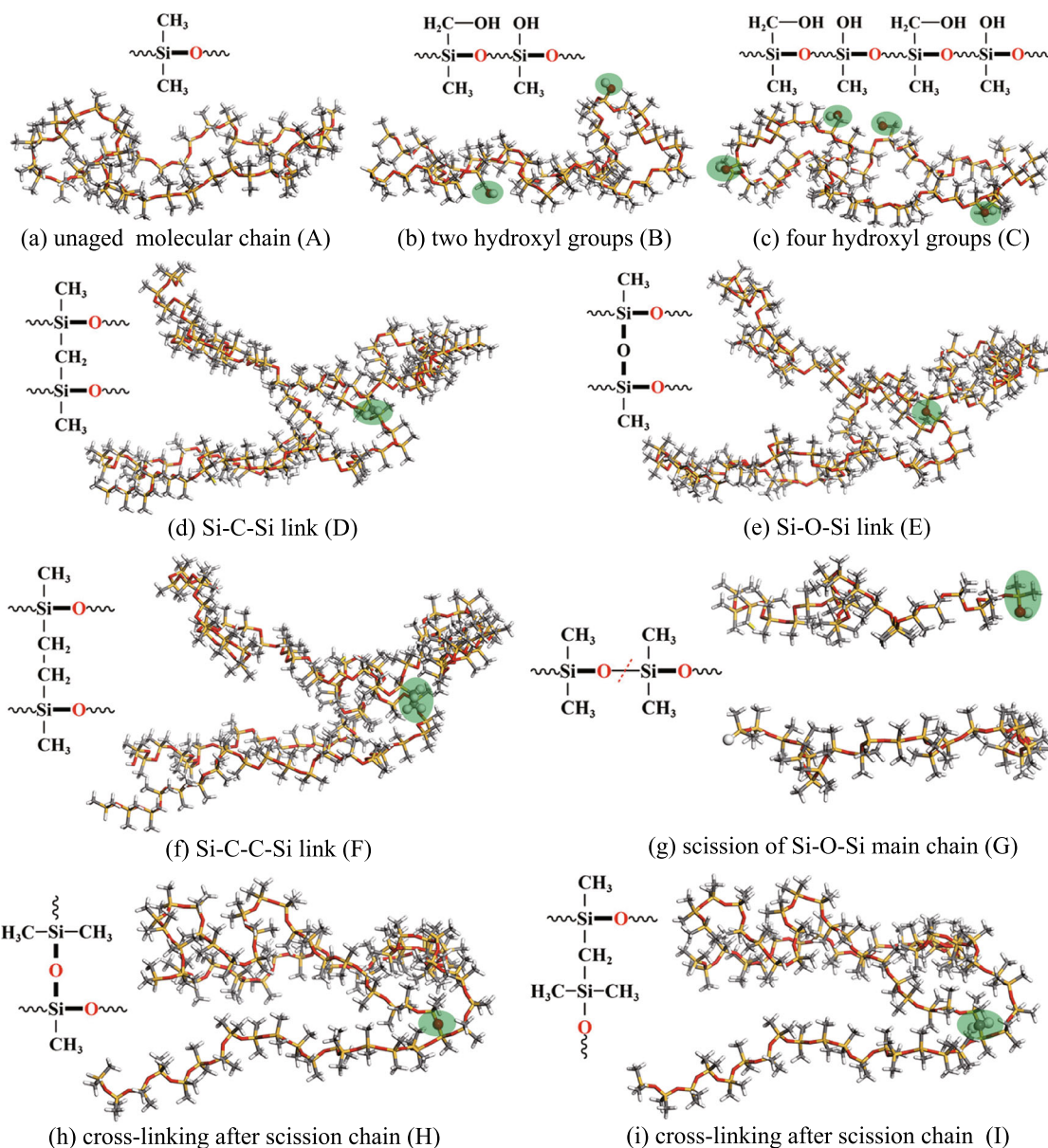


**Fig. 15** The typical chemical structures of the unaged and aged PDMS chains. **a** unaged chain **A**, **b** oxidized chain **B** with two hydroxyl groups, **c** oxidized chain **C** with four hydroxyl groups, **d** cross-linking structure of Si-C-Si link **d**, **e** cross-linking structure of Si-O-Si link **e**, **f** cross-linking structure of Si-C-C-Si link **f**, **g** scission structure **G** of Si-O-Si main chain, **h** cross-linking structure **f** after scission chain, and **i** cross-linking structure **i** after scission chain.

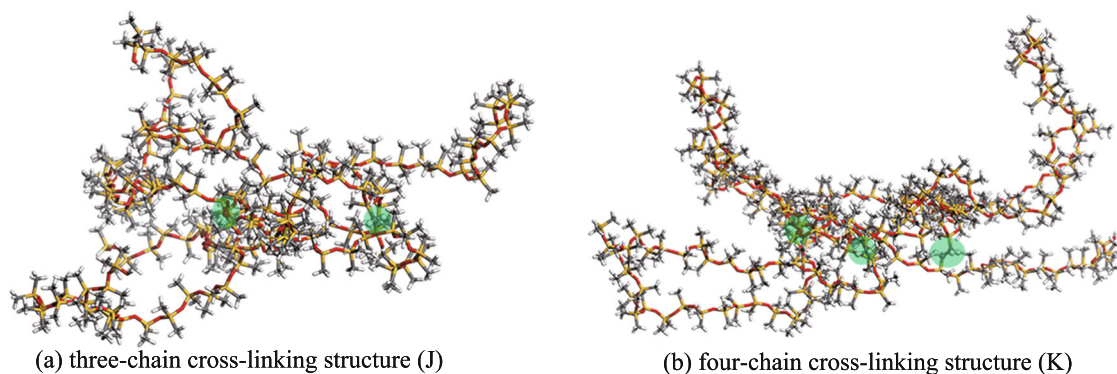


**Fig. 16** The typical multiple-chain cross-linking structures of the aged PDMS chains. **a** three-chain cross-linking structure (J) including Si-O-Si and Si-C-Si links and **b** four-chain cross-linking structure (K) including Si-O-Si, Si-C-Si, and Si-C-C-Si links.



**Table 2.** Details of the unaged and aged molecular models.

Molecular model	Number of chains										
	A	B	C	D	E	F	G	H	I	J	K
M1	20										
M2	4	16									
M3	4		16								
M4	4			8							
M5	4				8						
M6	4					8					
M7	4						16				
M8	4							4	4	4	
M9	4	2	2	1	1	1	3	1	1		
M10		1	1	2	2	2		2	2		
M11	5									5	
M12	4										4
M13		1	1		1		2			2	2

volume (FFV), hydrogen bonds (H-bonds), mean square displacement (MSD) and self-diffusion coefficients, radius of gyration, glass transition temperature, stress-strain curves, and diffusion behaviors of O<sub>2</sub> molecules were extracted from the resulting the equilibrated cells.

#### DATA AVAILABILITY

The data that support the findings of this study are available from the corresponding author upon reasonable request.

#### CODE AVAILABILITY

No code was used in this work.

Received: 5 May 2022; Accepted: 16 October 2022;

Published online: 29 October 2022

#### REFERENCES

- Wang, P. C. et al. Coupling effects of gamma irradiation and absorbed moisture on silicone foam. *Mater. Des.* **195**, 108998 (2020).
- Kaneko, T., Ito, S., Minakawa, T., Hirai, N. & Ohki, Y. Degradation mechanisms of silicone rubber under different aging conditions. *Polym. Degrad. Stabil.* **168**, 108936 (2019).
- Maiti, A., Gee, R. H., Weisgraber, T., Chinn, S. & Maxwell, R. S. Constitutive modeling of radiation effects on the permanent set in a silicone elastomer. *Polym. Degrad. Stabil.* **93**, 2226–2229 (2008).
- Roggero, A. et al. Inorganic fillers influence on the radiation-induced ageing of a space-used silicone elastomer. *Polym. Degrad. Stabil.* **128**, 126–133 (2016).
- Maiti, A. et al. Constitutive Model of Radiation Aging Effects in Filled Silicone Elastomers under Strain. *J. Phys. Chem. B.* **125**, 10047–10057 (2021).
- Chen, H. B., Liu, B., Huang, W. & Wu, W. H. Gamma radiation induced effects of compressed silicone foam. *Polym. Degrad. Stabil.* **114**, 89–93 (2015).
- Yan, S. et al. Influence of  $\gamma$ -irradiation on mechanical behaviors of poly methyl-vinyl silicone rubber foams at different temperatures. *Mech. Mater.* **151**, 103639 (2020).
- Liu, B. et al. Effects of combined neutron and gamma irradiation upon silicone foam. *Radiat. Phys. Chem.* **133**, 31–36 (2017).
- Celina, M., Linde, E., Brunson, D., Quintana, A. & Giron, N. Overview of accelerated aging and polymer degradation kinetics for combined radiation-thermal environments. *Polym. Degrad. Stabil.* **166**, 353–378 (2019).
- Wang, H. Y., Qiu, Y., Hu, W. J. & Chen, Y. M. Gamma radiation induced compressive response of silicon rubber foam: Experiments and modeling. *J. Mater. Res.* **34**, 2914–2200 (2019).
- Jia, D. et al. Constitutive modeling of  $\gamma$ -irradiated silicone rubber foams under compression and shear loading. *Polym. Degrad. Stabil.* **183**, 109410 (2021).

- Labouriau, A. et al. Coupled aging effects in nanofiber-reinforced siloxane foams. *Polym. Degrad. Stabil.* **149**, 19–27 (2018).
- Labouriau, A. et al. NMR and ATR-FTIR spectroscopic investigation of degradation in RTV siloxane foams. *Polym. Degrad. Stabil.* **92**, 414–424 (2007).
- Labouriau, A. et al. Aging mechanisms in RTV polysiloxane foams. *Polym. Degrad. Stabil.* **121**, 60–68 (2015).
- Maxwell, R. S., Cohenour, R., Sung, W., Solyom, D. & Patel, M. The effects of  $\gamma$ -radiation on the thermal, mechanical, and segmental dynamics of a silica filled, room temperature vulcanized polysiloxane rubber. *Polym. Degrad. Stabil.* **80**, 443–450 (2003).
- He, C. et al. How the crosslinking agent influences the thermal stability of RTV phenyl silicone rubber. *Materials* **12**, 88 (2018).
- Wu, J., Dong, J., Wang, Y. & Gond, B. K. Thermal oxidation ageing effects on silicone rubber sealing performance. *Polym. Degrad. Stabil.* **135**, 43–53 (2017).
- Tan, J. Z., Chao, Y. J., Li, X. D. & Van, J. W. Degradation of silicone rubber under compression in a simulated PEM fuel cell environment. *J. Power Sources* **172**, 782–789 (2014).
- Song, M., Zhao, X., Chan, T., Zhang, L. & Wu, S. Microstructure and dynamic properties analyses of hindered phenol AO-80/nitrile butadiene rubber/poly(vinyl chloride): a molecular simulation and experimental study. *Macromol. Theor. Simul.* **24**, 41–51 (2015).
- Zhao, X., Zhang, G., Lu, F., Zhang, L. & Wu, S. Molecular-level insight of hindered phenol AO-70/nitrile-butadiene rubber damping composites through a combination of a molecular dynamics simulation and experimental method. *Rsc. Adv.* **6**, 85994 (2016).
- Kroonblawd, M. P., Goldman, N., Maiti, A. & Lewicki, J. P. A quantum-based approach to predict primary radiation damage in polymeric networks. *J. Chem. Theory Comput.* **17**, 463–473 (2020).
- Liu, Q., Huang, W., Liu, B., Wang, P. C. & Chen, H. B. Gamma radiation chemistry of polydimethylsiloxane foam in radiation-thermal environments: experiments and simulations. *ACS Appl. Mater. Inter.* **13**, 41287–41302 (2021).
- Yu, K. Q., Li, Z. S. & Sun, J. Polymer structures and glass transition: a molecular dynamics simulation study. *Macromol. Theor. Simul.* **10**, 624–633 (2001).
- Xu, B., Wu, J. & McKenna, G. B. Mechanical and swelling behaviors of end-linked PDMS rubber and randomly cross-linked polyisoprene. *Macromolecules* **46**, 2015–2022 (2013).
- Hofmann, D., Fritz, L., Ulbrich, J., Schepers, C. & Böhning, M. Detailed-atomistic molecular modeling of small molecule diffusion and solution processes in polymeric membrane materials. *Macromol. Theor. Simul.* **9**, 293–327 (2000).
- Wang, X. et al. Artificial neural network modeling and mechanism study for relaxation of deformed rubber. *Ind. Eng. Chem. Res.* **55**, 4059–4070 (2016).
- Badenhoop, J. K. & Weinhold, F. Natural steric analysis: ab initio van der Waals radii of atoms and ions. *J. Chem. Phys.* **107**, 5422–5432 (1997).
- Brown, I. D. On the geometry of O–H... O hydrogen bonds. *Acta Crystallogr. A.* **32**, 24–31 (1976).
- Katrusiak, A. Stereochemistry and transformation of OH... O= hydrogen bonds Part I. Polymorphism and phase transition of 1, 3-cyclohexanedione crystals. *J. Mol. Struct.* **269**, 329–354 (1992).
- Zhu, L. et al. Tetraphenylphenyl-modified damping additives for silicone rubber: experimental and molecular simulation investigation. *Mater. Des.* **202**, 109551 (2021).
- Dong, C., Zheng, W., Wang, L., Zhen, W. & Zhao, L. Insight into glass transition temperature and mechanical properties of PVA/TRIS functionalized graphene oxide composites by molecular dynamics simulation. *Mater. Des.* **206**, 109770 (2021).
- Sheng, Y. Z., Yang, H., Li, J. Y. & Sun, M. Predicting glass transition temperature of polyethylene/graphene nanocomposites by molecular dynamic simulation. *Chem. Res. Chin. U.* **29**, 788–792 (2013).
- Ding, N., Chen, X., Wu, C. M. L. & Lu, X. Computational investigation on the effect of graphene oxide sheets as nanofillers in poly (vinyl alcohol)/graphene oxide composites. *J. Phys. Chem. C.* **116**, 22532–22538 (2012).
- Zhang, G., Sun, Y., Qian, B., Gao, H. & Zuo, D. Experimental study on mechanical performance of polydimethylsiloxane (PDMS) at various temperatures. *Polym. Test.* **90**, 106670 (2020).
- Sulyim, I., Klonos, P., Borysenko, M., Pissis, P. & Gun'ko, V. M. Dielectric and thermal studies of segmental dynamics in silica/PDMS and silica/titania/PDMS nanocomposites. *J. Appl. Polym. Sci.* **131**, 41154 (2014).
- Chen, E. Q. et al. Glass transition behavior of polystyrene blocks in the cores of collapsed dry micelles tethered by poly (dimethylsiloxane) coronae in a PS-b-PDMS diblock copolymer. *Chem. Mater.* **15**, 2129–2135 (2003).
- Li, Y., Vočadlo, L. & Brodholt, J. P. Elast: A toolkit for thermoelastic calculations. *Comput. Phys. Commun.* **273**, 108280 (2022).
- Souza, I. & Martins, J. Metric tensor as the dynamical variable for variable-cell-shape molecular dynamics. *Phys. Rev. B.* **55**, 8733 (1997).

39. Wu, C. L., Lin, H. C., Hsu, J. S., Yip, M. C. & Fang, W. Static and dynamic mechanical properties of polydimethylsiloxane/carbon nanotube nanocomposites. *Thin Solid Films*. **517**, 4895–4901 (2009).
40. Wei, Q., Wang, Y., Wang, S., Zhang, Y. & Chen, X. Investigating the properties and interaction mechanism of nano-silica in polyvinyl alcohol/polyacrylamide blends at an atomic level. *J. Mech. Behav. Biomed.* **75**, 529–537 (2017).
41. Xie, B. G. et al. A combined simulation and experiment study on polyisoprene rubber composites. *Compos. Sci. Technol.* **200**, 108398 (2020).
42. Hou, D., Yu, J. & Wang, P. Molecular dynamics modeling of the structure, dynamics, energetics and mechanical properties of cement-polymer nanocomposite. *Compos. Part B - Eng.* **162**, 433–444 (2019).
43. Parrinello, M. & Rahman, A. Strain fluctuations and elastic constants. *J. Chem. Phys.* **76**, 2662–2666 (1982).
44. Cox, M. E. & Dunn, B. Oxygen diffusion in poly (dimethyl siloxane) using fluorescence quenching. I. Measurement technique and analysis. *J. Polym. Sci. Polym. Chem.* **24**, 621–636 (1986).
45. Charati, S. G. & Stern, S. A. Diffusion of gases in silicone polymers: molecular dynamics simulations. *Macromolecules* **31**, 5529–5535 (1998).
46. Gillen, K. T. & Kudoh, H. Synergism of radiation and temperature in the degradation of a silicone elastomer. *Polym. Degrad. Stabil.* **181**, 109334 (2020).
47. Maiti, A., Gee, R. H. & Weisgraber, T. Modeling the Mechanical and Aging Properties of Silicone Rubber and Foam-Stockpile-Historical & Additively Manufactured Materials. (Lawrence Livermore National Lab., Livermore, United States, 2014).
48. Maiti, A. et al. Thermal aging of traditional and additively manufactured foams: analysis by time-temperature-superposition, constitutive, and finite-element models. (Lawrence Livermore National Lab., Livermore, United States, 2016).
49. Kroonblawd, M. P., Goldman, N. & Lewicki, J. P. Chemical degradation pathways in siloxane polymers following phenyl excitations. *J. Phys. Chem. B.* **122**, 12201–12210 (2018).
50. Lou, W., Xie, C. & Guan, X. Coupled effects of temperature and compressive strain on aging of silicone rubber foam. *Polym. Degrad. Stabil.* **195**, 109810 (2022).
51. Zhu, L. et al. Effects of chain structure on damping property and local dynamics of phenyl silicone rubber: Insights from experiment and molecular simulation. *Polym. Test.* **93**, 106885 (2021).
52. Koopman, E. A. & Lowe, C. P. Advantages of a lower-andersen thermostat in molecule dynamics simulations. *J. Chem. Phys.* **124**, 137 (2006).
53. Davoodi, J. & Ahmadi, M. Molecule dynamics simulation of elastic properties of CuPd nanowire. *Compos., Part B - Eng.* **43**, 10 (2012).

## ACKNOWLEDGEMENTS

This work was supported by 2020-JCJQ-JJ-465, CAEP, CX20200035, National Natural Science Foundation of China, Nos. U1930403, 12088101, and Science Challenge Project, No.TZ2018007. The support is gratefully acknowledged.

## AUTHOR CONTRIBUTIONS

W.L.: Methodology, Writing-Original Draft Preparation. C.X.: Methodology. X.G.: Writing—review & editing.

## COMPETING INTERESTS

The authors declare no competing interests.

## ADDITIONAL INFORMATION

**Correspondence** and requests for materials should be addressed to Xuefei Guan.

**Reprints and permission information** is available at <http://www.nature.com/reprints>

**Publisher's note** Springer Nature remains neutral with regard to jurisdictional claims in published maps and institutional affiliations.



**Open Access** This article is licensed under a Creative Commons Attribution 4.0 International License, which permits use, sharing, adaptation, distribution and reproduction in any medium or format, as long as you give appropriate credit to the original author(s) and the source, provide a link to the Creative Commons license, and indicate if changes were made. The images or other third party material in this article are included in the article's Creative Commons license, unless indicated otherwise in a credit line to the material. If material is not included in the article's Creative Commons license and your intended use is not permitted by statutory regulation or exceeds the permitted use, you will need to obtain permission directly from the copyright holder. To view a copy of this license, visit <http://creativecommons.org/licenses/by/4.0/>.

© The Author(s) 2022